In Silico Numerical Model of Aluminum and Iron Dissolution During Electric Pulse Application for Electroporation

Katja Balantič, PhD, Peter Kramar, PhD, and Damijan Miklavčič, PhD

Abstract

Introduction: Electroporation is a technique that increases the cell membrane permeability by application of electric pulses and has a widespread use in different fields such as medicine, biotechnology as well as in the food industry. Electric pulses unavoidable cause electrochemical reactions at the electrode–electrolyte interface among others, metal release from the electrodes. Consequently, a challenge in developing electroporation treatments is in predicting and optimizing the factors affecting electrochemical reactions. Efficient tool for optimization of electroporation protocols is by modeling the reactions that take place close to the electrodes.

Objectives: The aim of this work was to develop and validate a numerical model to describe electrochemical reactions, mainly metal dissolution taking place at the electrode–electrolyte interface during the application of electric pulses.

Methods: The analysis was focused on modeling aluminum cuvette and stainless steel plate electrodes, as they are commonly used in electroporation research. A two-dimensional model was used with Nernst–Planck equations for ion transport and Butler–Volmer equations to describe electrode kinetics thus for the first time giving the possibilityto implement different electroporation protocols, that is, pulse waveforms as an input function to the numericalmodel. The developed model was validated using experimental study by Kotnik et al.

Results: Numerical model shows that the pulse amplitude and polarity (monophasic vs. biphasic) greatly affects the dissolution of aluminum and iron ions from the electrodes.

Conclusions: The presented model requires further improvements but can with its limitations be used to optimize electroporation pulse waveforms in medicine and biology.

Keywords: electroporation, electrochemical reaction, numerical simulation, mathematical modeling

Introduction

EXPOSURE OF BIOLOGICAL cells to electric field has proven to be a useful tool for manipulating the cell membrane permeability and has a widespread use in many medical[1–4] and biotechnological applications[5,6] as well as in the food industry.[7] Even short-term exposure to electric field can induce structural changes in biological membranes owing to the formation of hydrophilic pores. As a result, the membrane becomes temporarily more permeable for molecules, which usually lack the mechanism to cross the membrane's hydrophobic barrier.[8] This phenomenon is known as electroporation.[9]

In medicine and biology, electroporation is used in numerous applications including electrochemotherapy,[10] gene therapy,[11] and tissue ablation.[12] When using reversible electroporation the cell remains viable after exposure to electrical pulses and is used primarily for introduction of chemotherapeutic drugs or genes into the cell. On the contrary, in irreversible electroporation (IRE), the membrane can reseal, but the cell dies nevertheless.[2] IRE is mainly used for tissue ablation of abdominal tumors and heart muscle.[3,13–15] It is believed that tissue destruction is caused mainly by necrosis and/or apoptosis.[16] Because of application of electric pulses, electrochemical reactions occur at the electrode–electrolyte interface, potentially contributing to cell death as

Faculty for Electrical Engineering, University of Ljubljana, Ljubljana, Slovenia.

suggested recently.[17–21] These reactions cause electrolysis, which results in pH changes, generation of radicals, and the release of metal ions from the electrodes, as well as formation of bubbles in the form of gaseous oxygen and hydrogen.[7,22]

Owing to the increasing use of electroporation in biology and medicine and in particular in intracardiac ablation,[13–15] it is important to carefully examine all possible electrochemical processes and thus ensure minimization of unwanted electrode chemical reactions to guarantee its safe and best use.

Electroporation can be electrochemically described as an application of electric pulses passing electric current through electrodes in contact with the tissue.[23] Application of electric pulses unavoidably causes electrochemical reactions at the electrode–electrolyte interface, specifically, metal release from the electrodes, which can have adverse effects on the electroporation process, equipment, and biological tissue. Aluminum cuvettes and stainless steel electrodes are commonly used in electroporation-based experiments and treatments.[24] However, aluminum is known to be toxic to the biological environment.[25–27] Excess iron ions can also lead to modifications of the cell membrane[28,29] and cause lipid oxidation.[30,31] What is more, electrochemical reactions also cause electrode wear owing to corrosion, and their surface roughness can increase because of metal dissolution.[32] This, in turn, can lead to distortions of the electric field and arcing, which shortens the lifetime of the electrodes.[33] Electrochemical reactions are therefore important aspect of electroporation process, but not well described yet.

Limited research is available on electrode's reactions and their consequences. It has been found that the amount of dissolved metal depends on the material of the electrode, and pulse parameters such as its shape, amplitude, polarity, and duration as well as the composition and chemical–physical properties of the electrolyte.[34–36] Different strategies are used to reduce the intensity of electrochemical reactions, for example, lowering the current and the conductance of the electrolyte, shortening the pulses, or use of biphasic pulses. Studies also showed that different pulse repetition rate affects the concentration of released metal ions.[22,37]

One possible tool for optimization of electroporation protocols is by modeling the electrochemical processes and reactions that take place close to the electrodes. Numerical models can be used to predict the course of electroporation, electrochemical processes occurring at the electrode–electrolyte interface, pH changes, and any possible side effects.[22,23,33,35,38] With a set of differential equations, we can describe electrochemical reactions and by solving these mathematical models, concentration profiles of dissolved substances and the potential profile can be simulated as a function of used electroporation protocol.[39–41]

The aim of this work was to develop a numerical model to describe electrochemical processes taking place at the electrode–electrolyte interface, for minimization of unwanted processes such as undesirable metal release from aluminum cuvettes[24,34,42,43] and from stainless steel electrodes[41,44–47] during electroporation. A two-dimensional (2D) numerical model was developed with Nernst–Planck equations for ion transport and Butler–Volmer equations to describe electrode kinetics. The model was solved with COMSOL Multiphysics (Comsol, Inc., Burlington, MA).[48] The results were compared with experimental data from the study of cell suspension contamination carried out by Kotnik et al.[34]

The emphasis of the study was on the use of two different electroporation protocols, namely monophasic and biphasic electric pulses, which were used in the model using COMSOL's built-in function. The study shows that not only the pulse amplitude but also the polarity of the electric pulses greatly influences the dissolution of metal ions. The model can be further used to study optimal electroporation parameters with the novel possibility to implement the electric pulse waveform as an input function to the numerical model. Specifically, we can use the pulse waveforms measured during experiments and treatments as an input function to the model.

Theory

Electroporation, that is, electric pulse delivery, can be represented as an electrochemical cell, where two or more electrodes are immersed in electrolyte.[38,49] Most often metals are used to build electrodes, consequently electric current flows through them via the movement of electrons. Once we place an electrode in the (aqueous) electrolyte, the movement of electrons in the electrodes is converted to the movement of ions in the electrolyte. Consequently an electrode–electrolyte interface will form, where electrical energy in the form of electrons is transferred to chemical energy in the form of ions.[45,50,51]

Two electrodes with different polarities and processes are distinguished, the positive anode where oxidation or loss of electrons takes place and the negative cathode where reduction or gain of electrons occurs. If NaCl is used as an aqueous electrolyte then anodic electrochemical reactions consist mainly of production of oxygen, gaseous chlorine and protons, whereas gaseous hydrogen and hydroxide ions are released at the cathode. This results in acidification (lowering pH) at the anode and alkalinization (increasing pH) at the cathode.[22,23,35,38] The most important electrochemical reactions at the anode are the oxygen evolution and chlorine evolution reactions:

$$2H_2O \leftrightarrow O_{2(g)} + 4H^+ + 4e^- \quad (1)$$

$$2Cl^- \leftrightarrow Cl_{2(g)} + 2e^- \quad (2)$$
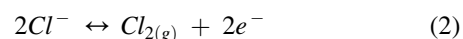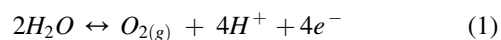
When using a metal electrode, the dissolution of the material from the anode occurs as well:

$$M_{(s)} \leftrightarrow M^{x+} + Xe^- \quad (3)$$
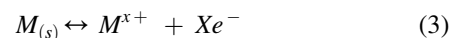
The main reaction at the cathode is the hydrogen evolution:

$$2H_2O + 2e^- \leftrightarrow H_{2(g)} + 2OH^- \quad (4)$$
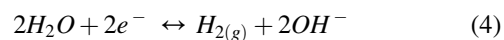
The only homogeneous chemical reaction in the electrolyte that is accounted for in our model is the water proteolysis reaction:

$$H^+ + OH^- \leftrightarrow H_2O. \quad (5)$$
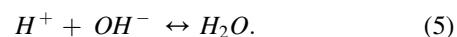
Important phenomenon of electrochemical cells is the so-called double layer.[52] Electric double layer refers to the region of charged particles that forms at the electrode–electrolyte interface even if no external voltage is applied. It consists of two layers: the first layer comprises ions that are

strongly attracted to the electrode surface and form a condensed layer, called the Stern layer; the second layer consists of ions that are less strongly attracted to the electrode surface and form a diffuse layer, called the Gouy–Chapman layer.[39] Once the potential drop across the double layer overcomes the threshold voltage of the reaction potential of electrode material, electrochemical reactions start to occur.[41,45]

The electrochemical reactions that occur at each of the two electrodes are also determined by the choice of material. When an electrochemically soluble material, such as aluminum,[53] is used, the majority of the anodic current results from the dissolution of the metal. Metal ions are then transported to the surrounding electrolyte, where they may produce harmful effects to cells, depending on the type of metal used.[23,36,42,49,53,54] The amount of chemical reactions and released metal ions is proportional to the charge in the form of electrons that is transferred across the electrode–electrolyte interface, during the oxidation or reduction, that is, to the amplitude and duration of the electric current. The metal ions and other ionic species released at the anode and cathode are transported to the surrounding electrolyte mainly by diffusion, owing to existing concentration gradients, and migration during the electric pulse, owing to electric potential gradient.[22,47]

Furthermore, the reaction products, specifically the H^+ and OH^- ions produced around the electrodes, are believed to be the main cause of tissue ablation by low-level direct current (electrochemical treatment) owing to electrolysis and strong changes in pH.[35,51,55,56] If one of the mechanism leading to cell death during electric pulse application is related to the electrochemical reactions at the electrode–electrolyte interface such as electrolysis, metal dissolution, and pH changes, then a numerical model describing these processes can be a useful tool to optimize the electroporation protocols. Such a model should be able to calculate concentration profiles of substances dissolved in the electrolyte as well as the potential profile in dependence of different electroporation parameters.[57]

Modeling

A finite element method–based software COMSOL Multiphysics 6.0 (Comsol, Inc.) with *Electrochemistry module* was used for all numerical computations. The electrochemical model consists of two electrodes, namely the anode and the cathode surrounded by the electrolyte as in previous studies.[23,35,51,58] The analysis was focused on a model of either aluminum cuvette or stainless steel plate electrodes, as they were used in the experiments we used for model validation.[34] As an approximation, the cell suspension was treated as an aqueous solution of 0.16 M NaCl at pH 7.

The following simplifications were used in the model, namely, convection was neglected. Also it was assumed that the gas bubbles formed on the electrode surface do not influence the overall conductivity of the electrolyte. The solution domain to the problem is the electrolyte phase, where

TABLE 1. INPUT PARAMETERS OF THE MATHEMATICAL MODEL

Name	Value	Description	Name	Value	Description
x	2 mm	Geometry x	z_Fe	2	Charge number, Fe
y	9 mm/11.3 mm	Geometry y	z_Al	3	Charge number, Al
D_Na	0.89^{-5} cm^2/s	Diffusivity, Na	z_OH	−1	Charge number, OH
*D*_H	$6.25e^{-5}$ cm^2/s	Diffusivity, H	i_I0	$1e^{-6}$ A/m^2	Exchange current density, reaction 1
D_Cl	$1.36e^{-5}$ cm^2/s	Diffusivity, Cl	i_II0	10 A/m^2	Exchange current density, reaction 2
D_Fe	$1.98e^{-5}$ cm^2/s	Diffusivity, Fe	i_III0	0.1 A/m^2	Exchange current density, reaction 3 Fe
D_OH	$3.52e^{-5}$ cm^2/s	Diffusivity, OH	i_III0	$1e^{-4}$ A/m^2	Exchange current density, reaction 3 Al
T	298 K	Temperature	i_IIII0	1 A/m^2	Exchange current density, reaction 4
Na0	0.16 M	Initial concentration, Na	E_eqI	1.23 V	Equilibrium potential, reaction H
H0	$1e^{-7}$ M	Initial concentration, H	E_eqII	1.36 V	Equilibrium potential, reaction Cl
Cl0	0.16 M	Initial concentration, Cl	E_eqIII	−0.44 V	Equilibrium potential, reaction Fe
Fe0	$1e^{-4}$ M	Initial concentration, Fe	E_eqIII	−1.66 V	Equilibrium potential, reaction Al
Al0	$1e^{-4}$ M	Initial concentration, Al	E_eqIIII	−0.828 V	Equilibrium potential, reaction OH
OH0	$1e^{-7}$ M	Initial concentration, OH	kf	$1.5e^{11}$ dm^3/(mol s)	Backward rate constant water hydrolysis
H2O0	55.5 M	Initial concentration H2O	kb	$2.7e^{-5}$ s^{-1}	Forward rate constant water hydrolysis
z_Na	1	Charge number, Na	z_Cl	−1	Charge number, Cl
*z*_H	1	Charge number, H	D_Al	$3.65e^{-5}$ cm^2/s	Diffusivity, Al

All input parameters were obtained from Nilsson et al.[23] For Al^{3+} and Fe^{2+} the values were obtained from Electrochemical Thermodynamics and Kinetics (Landolt-Börnstein: Numerical Data and Functional Relationships in Science and Technology).[61]

FIG. 1. Three-dimensional geometries that were converted to two-dimensional geometries used in the numerical model: **(A)** aluminum cuvette, h = 20 mm, y = 11.3 mm, x = 2 mm between the electrodes and **(B)** stainless steel electrodes with the corresponding dimensions: h = 20 mm. y = 9 mm, x = 2 mm between the electrodes.
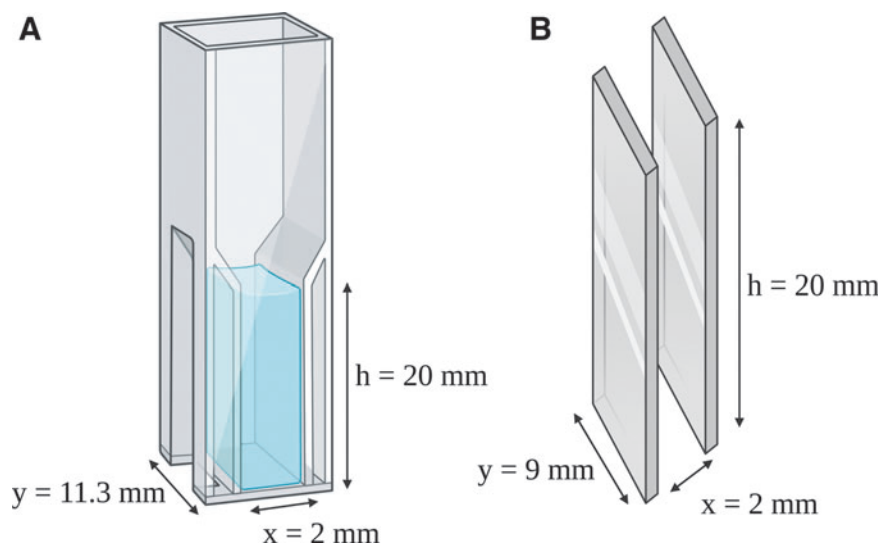
transport equations take place. There are two boundaries; the anode surface and the cathode surface, where reactions take place. All the kinetic parameters were obtained from the literature and can be found in Table 1. The transport equations and electrode kinetics used in the mathematical model are presented hereunder.

Geometry

The model consists of two *Rectangle* 2D geometries, the first geometry represents the aluminum cuvette (Fig. 1A), and the second geometry represents the stainless steel plate electrodes (Fig. 1B). The modeled 2D geometries are given in Figure 2.

Governing equations

The main equations used in the COMSOL numerical model are described hereunder. The COMSOL *Electrochemistry* module provides users with ready-made, user-friendly interface for modeling electrochemical processes. The model uses the *Tertiary current distribution, Nernst–Planck* interface to describe the transport and reactions during application of electric pulses. Using Nernst–Planck equation, the problem was solved for several variables, such as the concentration of individual ions, for example, Na$^+$, Cl$^-$, H$^+$, OH$^-$ and metal ions according to the material used for the

electrode in the model. Therefore, metal release can be described as a mass transport process using Nernst–Planck equation:

$$\frac{\partial c_i}{\partial t} = -\nabla N_i + R_i \tag{6}$$

where c_i is the concentration and R_i the reaction rate of the ionic species i. N_i is the molar flux of the ionic species i. Sodium-based electro-neutrality was used as a charge conservation model, for example, Na$^+$ concentration was obtained by Equation 7 where z_i is the valence number of the ion:

$$\sum_{i=1}^{5} z_i c_i = 0 \tag{7}$$

Transport of ionic species takes place by diffusion, owing to concentration gradients, and electric migration, caused by the presence of electric potential gradients. Therefore, the molar flux, N_i, of the ionic species i can be expressed as:

$$N_i = -D_i \nabla c_i - z_i u_i c_i \nabla \Phi \tag{8}$$

where D_i is the diffusion coefficient, u_i is the mobility and z_i is the number of charges carried by the ion i (valence number). Φ is the electric potential in the electrolyte, therefore, $\nabla \Phi$ is
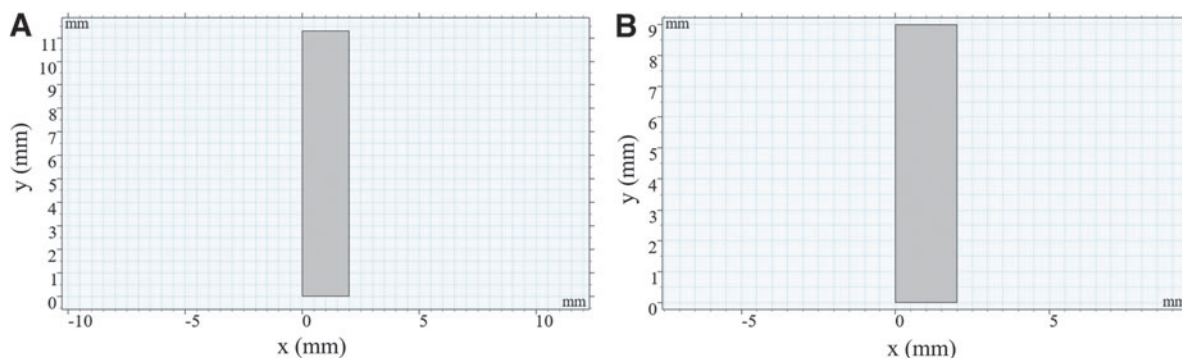
FIG. 2. Two-dimensional geometries implemented in the numerical model. **(A)** The two-dimensional rectangle geometry for aluminum cuvette and **(B)** stainless steel electrodes. The distance between the electrodes (x) was 2 mm in both cases.

electric field in electrolyte. Faradic current density, j in the electrolyte is calculated from the flux of charged species, and is given by Faraday's law:

$$j = F \sum_{i=1}^{5} z_i N_i \qquad (9)$$

where F is the Faraday constant. Therefore, the equation for conservation of electric charge $\nabla j = 0$, is used to solve the electric field:

$$\sum_{i=1}^{5} z_i D_i \nabla^2 c_i + \nabla \sum_{i=1}^{5} z_i u_i c_i \nabla \Phi = 0. \qquad (10)$$

In addition to the transport equations, kinetics of the electrode reactions are introduced at the anode and cathode boundary. The expressions for molar fluxes at the boundaries are based on the electrode reaction currents based in Equation 8 and Equation 9:

$$N_i = \frac{-v_i j_i}{nF} \qquad (11)$$

where v_i represents the stoichiometric coefficient, n the number of electrons transferred in the electrochemical reaction and j_i the Faradic current density for reaction i. The partial current density expression for each reaction was calculated using the *Butler–Volmer* type of kinetics expression with *From kinetics expression* option in COMSOL; therefore, the current density for electrochemical reactions is calculated as:

$$I = I_o \left(exp^{\left(\frac{\alpha a F z}{RT} \right)} - exp^{\left(\frac{\alpha c F z}{RT} \right)} \right) \qquad (12)$$

where I_o is the exchange current density. The first exponential term in Equation 12 represents the rate of the anodic process, whereas the second term is that of the cathodic process. αa and αc are the anodic and cathodic transfer coefficients, respectively. Transfer coefficients describe the likelihood of electrochemical reactions occurring at the electrodes. These coefficients are used in the framework of the Butler–Volmer equation, describing the relationship between the rate of the electrochemical reaction and the electrode potential. For reactions taking place at the anode (Equation 1, 2, 3) the αa was set to 1 and αc to 0. The same is true for reactions taking place at the cathode (Equation 4) where αc was 1 and αa was 0. R is the gas constant and T is temperature.

Electrodes were introduced as boundary conditions to the left and right side of the studied geometry. *Electrode surface* node was used to model anode and cathode with specific reactions. For upper and lower boundary condition, for example, insulation, there was no flux $-n*N_i = 0$ and no electric potential $-n*j_i = 0$. In the electrolyte, the *Reactions node* was used to model the water proteolysis reaction.

Electric potential was applied to the *Electrode surface* node as an *External electric potential* condition. Monophasic and biphasic electric pulses were used in the model. For eight monophasic pulses the pulse duration was 1 ms, frequency was 1 Hz. The electric pulse was obtained by subtracting two Heaviside functions using COMSOL's built in function *flc1hs*.[59,60] The pulse rise time was set to 0.001 ms to ease the

sharpness of the square pulse for better convergence of the model. The values of electric potential applied were from 40 V to 400 V.

For eight biphasic pulses, each pulse was of 1 ms total duration (500 μs of positive polarity followed by 500 μs of negative polarity). For biphasic pulses the electric pulse was obtained in a similar way to monophasic one. The positive polarity pulse was obtained subtracting two Heaviside functions using COMSOL's built-in function *flc1hs*. The negative polarity pulse was obtained by multiplying the positive one with (−1). The pulse rise time was set to 0.001 ms and the delay time between positive and negative pulse was 0.1 ms.[59,60] The polarities were exchanged in such a way that the first 500 μs of pulse was applied to the anode surface and the opposite polarity for the duration of 500 μs was applied to the cathode surface. In such a way, anodic reactions were exchanged for cathodic reactions midpulse. The values of electric potential applied were from 40 V to 280 V (peak-to-peak amplitude). The function of electric pulses was implemented in the *Definitions* section, under *Function*, *Analytic*.

Electrochemical reactions were applied to the anode (Equation 1, 2, and 3) and cathode (Equation 4) electrode surface. For each specific reaction the stoichiometric coefficients, equilibrium potential E_{eq} and electrode kinetics were applied. For the electrolyte reactions, the water proteolysis reaction was considered with the following reaction rates (Equation 13) for H^+ and OH^-.

$$R_H = R_{OH} = k_b \cdot c_{H_2O} - k_f \cdot c_H \cdot c_{OH} \qquad (13)$$

where, k_b and k_f are the rate constants of the water proteolysis reaction in the backward and forward direction.

Initial and boundary conditions

Inputs to the model are the electric potential, width (y) of the electrodes and the function to model the waveforms of monophasic and biphasic pulses. Thermodynamic and kinetic parameters used in the model are listed in Table 1. Standard electrode potentials are given relative to standard hydrogen electrode at 25°C. The partial pressures of oxygen and chlorine, produced at the anode, are assumed to be constant and equal to 1 atm.

Computational methods

The set of partial differential equations introduced in the previous paragraphs, with their relative initial and boundary conditions were solved using the commercial software package COMSOL Multiphysics 6.0 (Comsol, Inc.).

Events physics was used to solve the model. For monophasic pulses 6 explicit events were added to describe a single pulse, whereas for biphasic pulses 12 explicit events were added to describe a single pulse. The event was made periodic to include all eight pulses.

A user-defined mesh was implemented with custom element size. Mapped distribution with linear growth rate was used to discretize the electrolyte domain. Sufficiently dense boundary layer elements close to the electrodes was implemented to resolve the sharp concentration gradients and suppress oscillations in the electrolyte domain until no

further noticeable changes in the model results were observed. Number of elements was 200 and element ratio was 400.

A time-dependent study with current distribution initialization was used to solve the equations. The studied time range was 9 s, with 0.0001 s time-step. A user-controlled tolerance was used with relative tolerance 0.0001. All the simulations were performed using a PC running on Windows 10 with Intel® Core™ i5-8259U CPU @ 2.30 GHz with 16 GB RAM, which allowed for solving the model in ∼10 min computation time.

Model validation

The experimental data for metal release used to validate the model was found in the study by Kotnik et al.[34] In the experimental study, the contamination of cell growth medium during application of electroporation pulses with varying voltage and pulse polarities was measured. A mass spectrometry analysis of the cell growth medium was carried out to obtain the concentration of released aluminum and iron ions.[34] The concentration values from the experimental study were obtained from the corresponding graphs using "graph reader" application. To obtain the concentration (mM) of the released metal ions from the COMSOL numerical model, the surface integration of the electrolyte domain was performed for each specific concentration of studied ions. Surface integration was performed using *Derived values* option in COMSOL. The obtained values for each specific ion concentration were then multiplied by the domain height (h) and divided by the electrolyte volume (50 μL) as used in the study by Kotnik et al.[34]

Results and Discussion

The time-dependent numerical model of electrochemical reactions at the electrode–electrolyte interface during the application of electric pulses was developed to observe the release of metal ions, for example, aluminum and iron from the electrodes, using different pulse waveforms functions as input parameters to the model. By applying the transport equations of ionic species in dilute solutions, and the equations of electrode kinetics, concentration profiles of metal ions and potential distribution were calculated as functions of used pulse waveforms.

Pulse waveform function, used in the model was either 8×1 ms monophasic pulses with frequency of 1 Hz as given in Figure 3A or 8×1 ms (500 μs positive followed by 500 μs negative) biphasic pulses with frequency of 1 Hz as given in Figure 3B. Voltage was varied from 40 V to 400 V for monophasic pulses and from 40 V to 280 V for biphasic pulses in the *Electrode surface* node that was set as the boundary condition in the model.

The spatial concentration profiles for Na^+, Cl^-, H^+, and OH^- are given in Figure 4 and were obtained as a "cut-line 2D" datasets in COMSOL. For better visualization of the concentration profiles in Figures 4, 5, and 6, the diffusivity was multiplied by a factor of 10^3 in the *Electrolyte, Diffusion* section of the model. Na^+ ions are depleted close to the positive anode surface, because it repels positive ions. At the cathode, the concentration of Na^+ ions increases because the positive ions move toward the negative electrode (Fig. 4A). There is no reaction for Na^+ ions in the model; therefore, their concentration remains constant throughout the simulation. Negatively charged chloride ions move toward the positive anode and away from negative cathode (Fig. 4B).
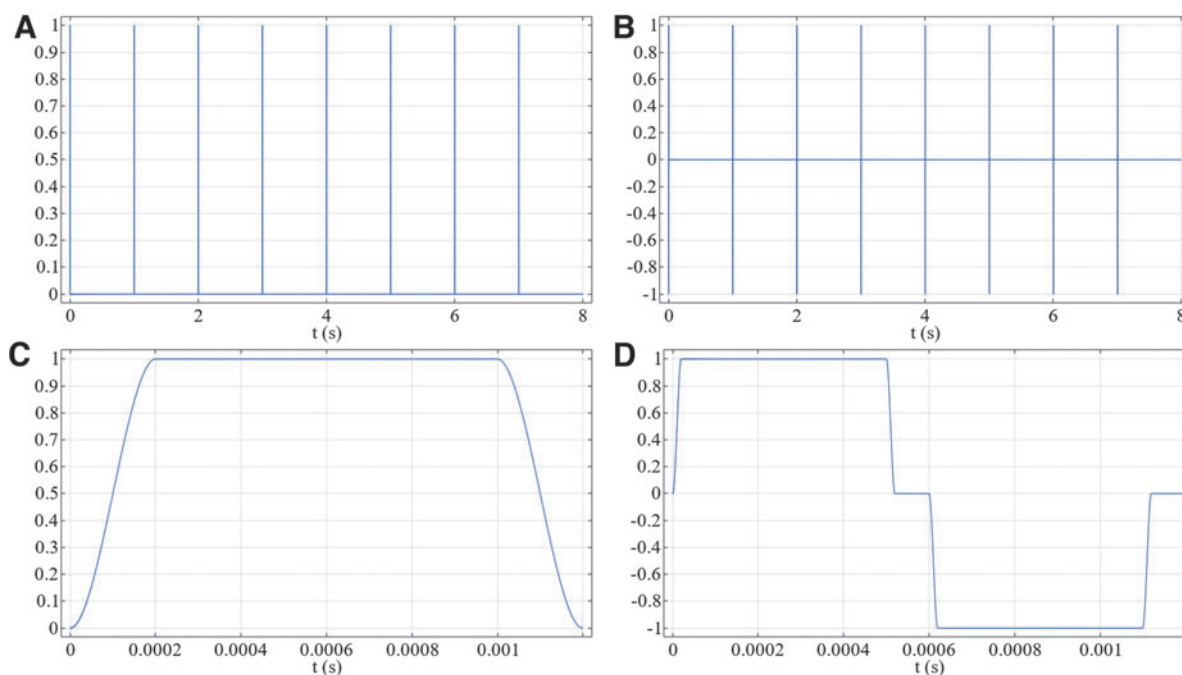
FIG. 3. Pulse waveform function used in the model. **(A)** The graph shows the function for monophasic pulses, which was applied to the anode surface and multiplied with the corresponding voltage (40 V–400 V). **(B)** The graph shows the function for biphasic pulses, where positive pulse was applied to the anode and negative pulse to the cathode and multiplied with the corresponding voltage (40 V–280 V). **(C)** A single monophasic pulse function. **(D)** A single biphasic pulse function.
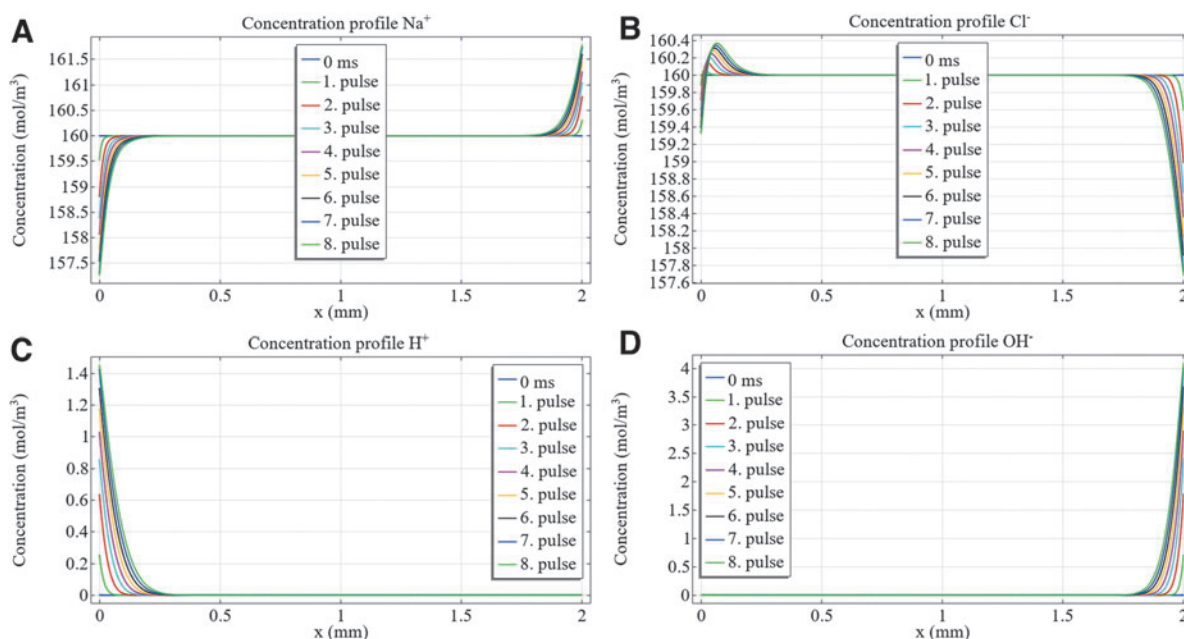
FIG. 4. Simulated **(A)** Na$^+$, **(B)** Cl$^-$, **(C)** H$^+$, and **(D)** OH$^-$ concentration (mM) versus distance (mm) after each monophasic pulse application. Applied voltage = 40 V. Spatial coordinate, x component presents the anode surface at 0 and cathode at 2 mm. For better visualization of the graphs, the diffusivity was multiplied by a factor of 10^3.

In the simulation Cl$^-$ are reactants in the chlorine evolution reactions, therefore their concentration decreases over time. Positive H$^+$ is a product of the oxygen evolution reactions at the anode, whereas negative OH$^-$ is a product of hydrogen evolution reaction at the cathode. H$^+$ and OH$^-$ concentration at the corresponding electrode surface increases (Fig. 4C, D).

With the known concentration of produced H$^+$ and OH$^-$ ions, a pH profile of the electrolyte domain can be obtained as a function of distance between the anode and the cathode. The pH profile is given in Figure 5. Acidic pH develops close to the anode, whereas alkaline pH develops close to the cathode.

Dissolution of metal ions

As the voltage applied in the numerical model reaches the threshold value of the reaction potential of electrode material and is higher than the equilibrium potential the dissolution of metal ions starts to occur. With increasing voltage, an increase in concentration of released metal was observed. The

highest concentration of released metal ions was observed as expected, for the highest pulse amplitude, that is, 400 V pulses. Figure 6 presents how the dissolution of (A) aluminum and (B) iron ions takes place after each 40 V pulse application. Figure 6C and D show the release of metal ions when pulses with amplitude of 400 V were applied. The concentration of released aluminum ions is slightly higher than of iron ions because more electrons play a role in the electrochemical reaction of aluminum dissolution and is in line with the experimental results. Since the anode is positively charged, the concentration profiles of positive metal ions moves away from the anode toward the negative cathode owing to diffusion in between the pulses and migration in electric field during the pulses.

To compare numerical results with the experimental values the molar concentration (mM) of the released metal ions was calculated. First, a concentration surface integral was calculated over the modeled geometry. The surface integral value was then multiplied by the height (h) of the electrodes to obtain the amount of released metal ions in moles. The
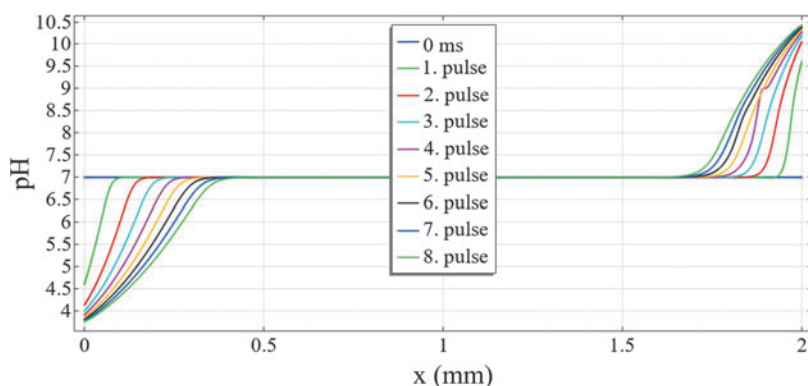
FIG. 5. Simulation of the pH profile for monophasic pulses. As the H+ ions are produced at the anode, the pH decreases to a more acidic value. On the contrary, at the cathode, OH$^-$ ions are produced, therefore the pH increases to a more alkaline value. Small oscillations can be seen on the cathode side, which could be owing to the pH calculation. Applied voltage = 40 V. For better visualization of the graphs, the diffusivity was multiplied by a factor of 10^3.
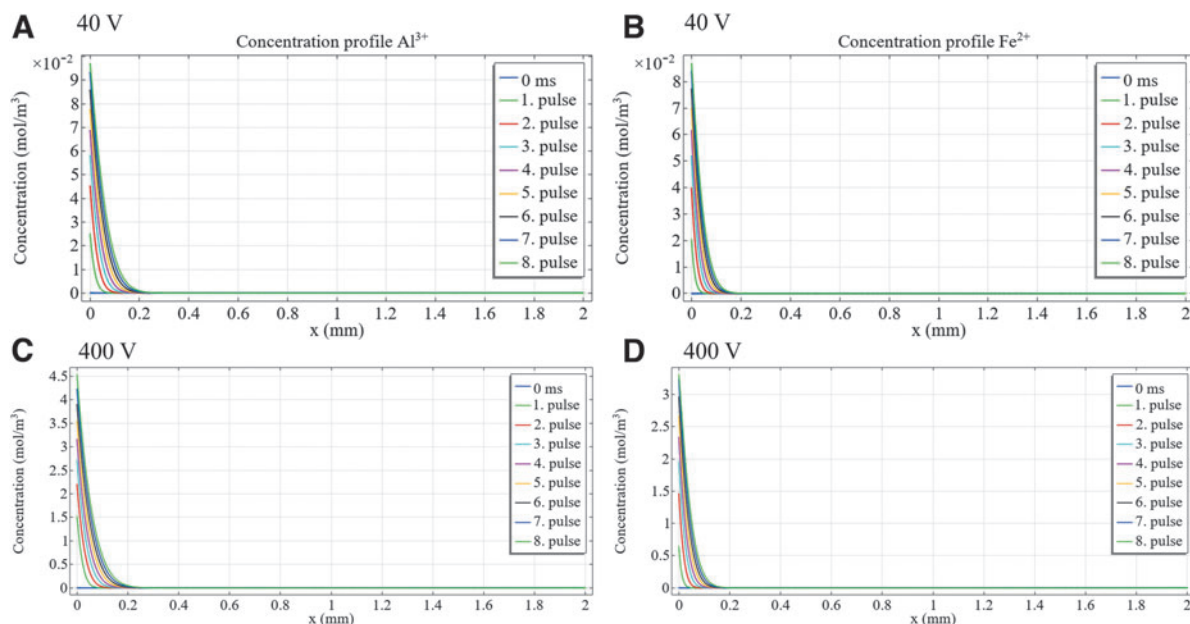
FIG. 6. Concentration of released metal ions for **(A)** aluminum and **(B)** iron as a function of distance from the anode after each monophasic pulse with applied voltage $=40$ V. **(C)** and **(D)** Concentration profiles of aluminum and iron ions after application of 400 V monophasic pulses. Spatial coordinate, x component presents the anode surface at 0 and cathode at 2 mm. For better visualization of the graphs, the diffusivity was multiplied by a factor of 10^3.

obtained values were then divided by the volume (50 μL) used in the experiments by Kotnik et al.[34] As the pulse amplitude increases, the energy for the electrochemical reactions is higher leading to a higher concentration of released metal ions.

Biphasic pulses were also used in the numerical model. As a first approximation, the biphasic pulse function was applied to the anode for the positive polarity (500 μs) and to the cathode for the negative polarity (500 μs). Therefore, the anodic and cathodic chemical reactions were interchanged during the simulation to model biphasic pulse application. Increase in the dissolved metal ions was observed for both aluminum and iron ions, with increasing biphasic pulse amplitude. However, metal release with biphasic pulses compared with monophasic ones was five times lower for aluminum and almost four times lower for iron ions. Of interest, for higher amplitudes both Al^{3+} and Fe^{2+} dissolution obtained from the model compare well at low amplitudes for both monophasic and biphasic pulses (Figs. 7 and 8) but deviates from experimental values for monophasic pulses.

Model validation

Modeled numerical results were compared with other peer-review numerical studies found in the literature. Specifically, the accuracy of the equations and input parameters for each electrode reaction was verified. The spatial concentration profiles for Na^+, Cl^-, H^+, and OH^- were also compared with the ones found in previous studies, to make sure the physics of our model is indeed correct.[23,51,55]

Model results were then compared with the experimental data published in a study by Kotnik et al.[34] and numerical representation of results is given in Supplementary Data in Tables S1 and S2. Good agreement between experimental and simulated data can be observed for monophasic pulse voltages <160 V as given in Figure 7. However, as the voltage of the applied pulses increases our numerical model apparently no longer adequately describes all the reactions taking place, therefore, the concentration of released metal ions in the model is lower than the one obtained in the experiments.
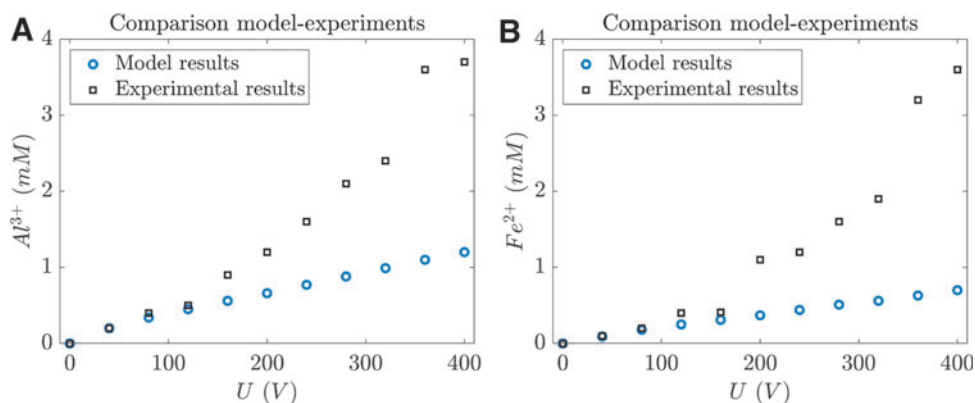
FIG. 7. Comparison of the simulated metal release data for monophasic pulses with the experimental data from Kotnik et al.[34] for **(A)** aluminum and **(B)** iron ions.
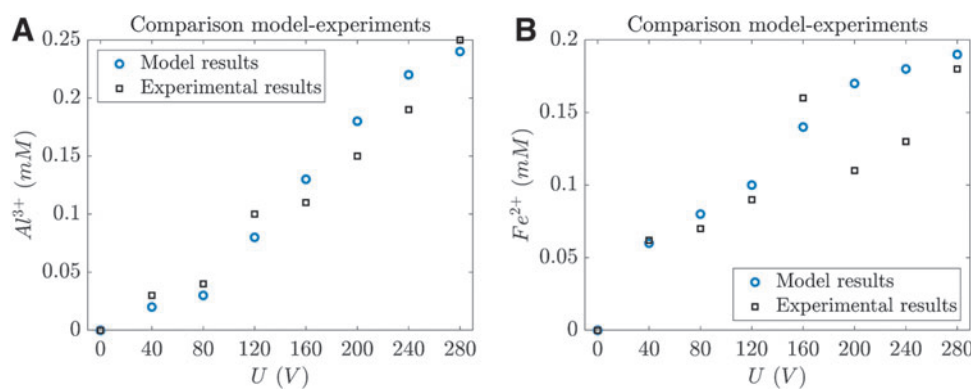
FIG. 8. Comparison of the simulated metal release data for biphasic pulses with the experimental data from Kotnik et al.[34] for **(A)** aluminum and **(B)** iron ions.

Discrepancies between numerical and experimental results at higher voltages (>200 V) could be because of additional electrochemical processes taking place at the electrode–electrolyte interface that are not accounted for in the presented numerical model. For example, the roughness of the electrode surface increases with dissolution of metal ions and corrosion; therefore, a larger surface is exposed to the electrolyte during the experiments, possibly leading to a higher concentration of released metal ions.[22,32] Furthermore, metal ions can react with other compounds in the electrolyte. Passivation and activation of aluminum electrode occurs depending on the applied potential, the pH, and Cl^- concentration. It has been shown that that higher pH and Cl^- concentration increase the anodic reaction rates and consequently concentration of released aluminum.[53,62] Experimental studies suggest that when aluminum electrodes are used, a cathode dissolution of Al^{3+} can also occur owing to a chemical attack of OH^- ions.[63]

Finally, the chloride ions present in the solution can also attack the stainless steel electrode and cause continuous dissolution of iron through pitting corrosion.[64] What is more, Fe^{2+} ions undergo iron oxidation to form Fe^{3+} in the presence of chlorine.[65] In the experimental study,[34] Fe^{2+} as well as Fe^{3+} ions were detected (because of analytical method used), resulting in higher release iron concentration in the experimental study. Metal ions released from the anode might also increase medium conductivity[54] leading to higher currents in the electrolyte that would increase the concentration of released metals. Furthermore, stainless steel is an iron alloy; therefore, it usually consists of not only iron, but also chromium, copper, nickel, manganese, and other metals, which are not accounted for in our model and could lead to additional electrochemical reactions.

Furthermore, apart from water proteolysis reaction, electrolyte reactions are not modeled in our simulation and could explain the differences between the experimental and modeled values. In addition, pH changes have an effect on higher release of metal ions, which is not accounted for in our model. What is more, in the experiments, the cell growth medium was studied, which could result in additional electrochemical reactions, owing to complex composition of the medium, compared with the one used in the model, where NaCl suspension was modeled.

Of interest, the modeled concentration of dissolved metal fits the experimental results much better, when biphasic pulses are used (Fig. 8). The amplitude for biphasic pulses was modeled as peak-to-peak value; therefore, the single electrode–electrolyte voltages were lower, leading to better correlation between numerical and experimental results.

The modeled dissolution of aluminum ions for biphasic pulses (Fig. 8A) is in good agreement with the experimental results for pulse amplitudes up to 120 V, followed by a slight overestimation of the modeled results for higher amplitudes. Similarly, the agreement between model and experimental results for iron dissolution with biphasic pulses (Fig. 8B) is good for amplitudes up to 160 V, whereas at higher amplitudes the model shows a higher release of metal ions as the one obtained in experiments.

Overall, we were able to develop a numerical model for description of electrochemical reactions and metal dissolution from aluminum cuvettes and iron electrodes during application of monophasic and biphasic electric pulse waveforms. However, the presented model would need further improvements to sufficiently describe the metal dissolution at higher voltages as well. Additional electrochemical reactions at the electrode–electrolyte interface should be identified and modeled, as well as secondary reactions of released aluminum and iron ions in the electrolyte. Nevertheless, with the given model, fewer experimental studies would be required for optimization of electroporation pulses protocols to achieve lower metal dissolution.

Conclusion

Electrochemical numerical models are important for a better understanding of reactions occurring at the electrode–electrolyte interface during the application of electric pulses. In our study, we developed a numerical model to describe dissolution of aluminum and iron ions at the electrode–electrolyte interface during application of 8×1 ms monophasic and biphasic pulses. The monophasic and biphasic electric pulse waveforms were introduced in the model as input parameters, thus providing the possibility to study the metal release in dependence of different pulse protocols with varying interphase and interpulse delays. We were able to validate the model using experimental result published in the article by Kotnik et al.[34] However, the model also showed a lack of complete description of electrochemical reactions at amplitudes higher than 160 V.

The numerical model therefore still needs further development, such as the introduction of additional electrochemical reactions at the electrode–electrolyte interface, secondary reactions in the electrolyte, and pH-induced modifications. Nevertheless, the developed and validated numerical model can be in principle used for optimization of protocols used in electroporation-based technologies and treatments.

Author Disclosure Statement

The authors declare that they have no known competing financial interests or personal relationships that could have influence the work reported in this article.

Funding Information

Supplementary Material

Supplementary Data
Supplementary Table S1
Supplementary Table S2

References

1. Miklavčič D, Mali B, Kos B, et al. Electrochemotherapy: From the drawing board into medical practice. Biomed Eng OnLine 2014;13(1):29; doi: 10.1186/1475-925X-13-29

2. Davalos RV, Mir ILM, Rubinsky B. Tissue ablation with irreversible electroporation. Ann Biomed Eng 2005;33(2): 223–231; doi: 10.1007/s10439-005-8981-8

3. Geboers B, Scheffer HJ, Graybill PM, et al. High-voltage electrical pulses in oncology: Irreversible electroporation, electrochemotherapy, gene electrotransfer, electrofusion, and electroimmunotherapy. Radiology 2020;295(2):254–272; doi: 10.1148/radiol.2020192190

4. Sugrue A, Maor E, Ivorra A, et al. Irreversible electroporation for the treatment of cardiac arrhythmias. Expert Rev Cardiovasc Ther 2018;16(5):349–360; doi: 10.1080/14779072.2018.1459185

5. Rosazza C, Haberl Meglic S, Zumbusch A, et al. Gene electrotransfer: A mechanistic perspective. Curr Gene Ther 2016;16(2):98–129; doi: 10.2174/1566523216666160331130040

6. Kotnik T, Frey W, Sack M, et al. Electroporation-based applications in biotechnology. Trends Biotechnol 2015;33(8):480–488; doi: 10.1016/j.tibtech.2015.06.002

7. Mahnič-Kalamiza S, Vorobiev E, Miklavcic D. Electroporation in food processing and biorefinery. J Membr Biol 2014;247(12):1279–1304; doi: 10.1007/s00232-014-9737-x

8. Kotnik T, Rems L, Tarek M, et al. Membrane electroporation and electropermeabilization: Mechanisms and models. Annu Rev Biophys 2019;48(1):63–91; doi: 10.1146/annurev-biophys-052118-115451

9. Kotnik T, Kramar P, Pucihar G, et al. Cell membrane electroporation- Part 1: The phenomenon. IEEE Electr Insul Mag 2012;28(5):14–23; doi: 10.1109/MEI.2012.6268438

10. Cemazar M, Sersa G. Recent advances in electrochemotherapy. Bioelectricity 2019;1(4):204–213; doi: 10.1089/bioe.2019.0028

11. Sachdev S, Potočnik T, Rems L, et al. Revisiting the role of pulsed electric fields in overcoming the barriers to in vivo gene electrotransfer. Bioelectrochemistry 2022;144:107994; doi: 10.1016/j.bioelechem.2021.107994

12. Cindrič H, Kos B, Miklavčič D. Ireverzibilna elektroporacija kot metoda ablacije mehkih tkiv: Pregled in izzivi pri uporabi v kliničnem okolju. Slov Med J 2021;90(1–2):38–53; doi: 10.6016/ZdravVestn.2954

13. Stewart MT, Haines DE, Miklavčič D, et al. Safety and chronic lesion characterization of pulsed field ablation in a Porcine model. J Cardiovasc Electrophysiol 2021;32(4): 958–969; doi: 10.1111/jce.14980.

14. Sugrue A, Vaidya V, Witt C, et al. Irreversible electroporation for catheter-based cardiac ablation: A systematic review of the preclinical experience. J Interv Card Electrophysiol 2019;55(3):251–265; doi: 10.1007/s10840-019-00574-3

15. Maor E, Ivorra A, Mitchell JJ, et al. Vascular smooth muscle cells ablation with endovascular nonthermal irreversible electroporation. J Vasc Interv Radiol 2010;21(11): 1708–1715; doi: 10.1016/j.jvir.2010.06.024

16. Batista Napotnik T, Polajžer T, Miklavčič D. Cell death due to electroporation–A review. Bioelectrochemistry 2021;141:107871; doi: 10.1016/j.bioelechem.2021.107871

17. Lv Y, Zhang Y, Rubinsky B. Molecular and histological study on the effects of electrolytic electroporation on the liver. Bioelectrochemistry 2019;125:79–89; doi: 10.1016/j.bioelechem.2018.09.007

18. Rubinsky L, Guenther E, Mikus P, et al. Electrolytic effects during tissue ablation by electroporation. Technol Cancer Res Treat 2016;15(5):NP95–NP103; doi: 10.1177/1533034615601549

19. Phillips M, Rubinsky L, Meir A, et al. Combining electrolysis and electroporation for tissue ablation. Technol Cancer Res Treat 2015;14(4):395–410; doi: 10.1177/1533034614560102

20. Bardy GH, Coltorti F, Ivey TD, et al. Some factors affecting bubble formation with catheter-mediated defibrillator pulses. Circulation 1986;73(3):525–538; doi: 10.1161/01.CIR.73.3.525

21. Perkons NR, Stein EJ, Nwaezeapu C, et al. Electrolytic ablation enables cancer cell targeting through pH modulation. Commun Biol 2018;1(1):48; doi: 10.1038/s42003-018-0047-1

22. Saulis G, Rodaitė-Riševičienė R, Dainauskaitė VS, et al. Electrochemical Processes During High-Voltage Electric Pulses and Their Importance in Food Processing Technology. In: Advances in Food Biotechnology. (Ravishankar RV. ed.) John Wiley & Sons, Ltd.: Hoboken, NJ; 2016; pp. 575–592.

23. Nilsson E, Berendson J, Fontes E. Electrochemical treatment of tumours: A simplified mathematical model. J Electroanal Chem 1999;460(1):88–99; doi: 10.1016/S0022-0728(98)00352-0

24. Friedrich U, Stachowicz N, Simm A, et al. High efficiency electrotransfection with aluminum electrodes using microsecond controlled pulses. Bioelectrochem Bioenerg 1998;47(1):103–111; doi: 10.1016/S0302-4598(98)00163-9

25. Abreo K, Glass J. Cellular, biochemical, and molecular mechanisms of aluminium toxicity. Nephrol Dial Transplant 1993;8(Supp1):5–11; doi: 10.1093/ndt/8.supp1.5

26. Crisponi G, Fanni D, Gerosa C, et al. The meaning of aluminium exposure on human health and aluminium-related diseases. Biomol Concepts 2013;4(1):77–87; doi: 10.1515/bmc-2012-0045

27. Exley C, Derek Birchall J. The cellular toxicity of aluminium. J Theor Biol 1992;159(1):83–98; doi: 10.1016/S0022-5193(05)80769-6

28. Saulis G, Rodaitė-Riševičienė R, Saulė R. Cytotoxicity of a cell culture medium treated with a high-voltage pulse using stainless steel electrodes and the role of iron ions. Membranes 2022;12(2):184; doi: 10.3390/membranes12020184

29. Sousa L, Oliveira MM, Pessôa MTC, et al. Iron overload: Effects on cellular biochemistry. Clin Chim Acta 2020;504: 180–189; doi: 10.1016/j.cca.2019.11.029

30. Lapidot T, Granit R, Kanner J. Lipid peroxidation by "Free" iron ions and myoglobin as affected by dietary antioxidants in simulated gastric fluids. J Agric Food Chem 2005;53(9):3383–3390; doi: 10.1021/jf040402g

31. Yamamoto Y, Hachiya A, Matsumoto H. Oxidative damage to membranes by a combination of aluminum and iron in suspension-cultured tobacco cells. Plant Cell Physiol 1997;38(12):1333–1339; doi: 10.1093/oxfordjournals.pcp.a029126

32. Mahnič-Kalamiza S, Miklavčič D. Scratching the electrode surface: Insights into a high-voltage pulsed-field application from in vitro & in silico studies in indifferent fluid. Electrochim Acta 2020;363:137187; doi: 10.1016/j.electacta.2020.137187

33. Pataro G, Donsì G, Ferrari G. Modeling of Electrochemical Reactions During Pulsed Electric Field Treatment. In: Handbook of Electroporation. (Miklavcic D. ed) Springer International Publishing: Cham, 2016; pp. 1–30.

34. Kotnik T, Miklavčič D, Mir LM. Cell membrane electropermeabilization by symmetrical bipolar rectangular pulses: Part II. Reduced electrolytic contamination. Bioelectrochemistry 2001;54(1):91–95; doi: 10.1016/S1567-5394(01)00115-3

35. Turjanski P, Olaiz N, Abou-Adal P, et al. pH front tracking in the electrochemical treatment (EChT) of tumors: Experiments and simulations. Electrochim Acta 2009;54(26):6199–6206; doi: 10.1016/j.electacta.2009.05.062

36. Saulis G, Rodaitė-Riševičienė R, Snitka V. Increase of the roughness of the stainless-steel anode surface due to the exposure to high-voltage electric pulses as revealed by atomic force microscopy. Bioelectrochemistry 2007;70(2):519–523; doi: 10.1016/j.bioelechem.2006.12.003

37. Vižintin A, Vidmar J, Ščančar J, et al. Effect of interphase and interpulse delay in high-frequency irreversible electroporation pulses on cell survival, membrane permeabilization and electrode material release. Bioelectrochemistry 2020;134:107523; doi: 10.1016/j.bioelechem.2020.107523

38. Pataro G. On the modeling of electrochemical phenomena at the electrode-solution interface in a PEF treatment chamber: Methodological approach to describe the phenomenon of metal release. J Food Eng 2015;165:34–44.

39. Richardson G, King JR. Time-dependent modelling and asymptotic analysis of electrochemical cells. J Eng Math 2007;59(3):239–275; doi: 10.1007/s10665-006-9114-6

40. Nilsson E, von Euler H, Berendson J, et al. Electrochemical treatment of tumours. Bioelectrochemistry 2000;51(1):1–11; doi: 10.1016/S0302-4598(99)00073-2

41. Pataro G, Barca GMJ, Pereira RN, et al. Quantification of metal release from stainless steel electrodes during conventional and pulsed ohmic heating. Innov Food Sci Emerg Technol 2014;21:66–73; doi: 10.1016/j.ifset.2013.11.009

42. Loomis-Husselbee JW, Cullen PJ, Irvine RF, et al. Electroporation can cause artefacts due to solubilization of cations from the electrode plates. Aluminum ions enhance conversion of inositol 1,3,4,5-tetrakisphosphate into inositol 1,4,5-trisphosphate in electroporated L1210 cells. Biochem J 1991;277(3):883–885; doi: 10.1042/bj2770883

43. Saulis G, Lapė R, Pranevičiūtė R, et al. Changes of the solution pH due to exposure by high-voltage electric pulses. Bioelectrochemistry 2005;67(1):101–108; doi: 10.1016/j.bioelechem.2005.03.001

44. Stapulionis R. Electric pulse-induced precipitation of biological macromolecules in electroporation. Bioelectrochem Bioenerg 1999;48(1):249–254; doi: 10.1016/S0302-4598(98)00206-2

45. Morren J, Roodenburg B, de Haan SWH. Electrochemical reactions and electrode corrosion in pulsed electric field (PEF) treatment chambers. Innov Food Sci Emerg Technol 2003;4(3):285–295; doi: 10.1016/S1466-8564(03)00041-9

46. Pataro G, Falcone M, Donsì G, et al. Metal release from stainless steel electrodes of a PEF treatment chamber: Effects of electrical parameters and food composition. Innov Food Sci Emerg Technol 2014;21:58–65.

47. Roodenburg B, Morren J, Berg HE (Iekje), et al. Metal release in a stainless steel pulsed electric field (PEF) system. Innov Food Sci Emerg Technol 2005;6(3):337–345; doi: 10.1016/j.ifset.2005.04.004

48. Dickinson EJF, Ekström H, Fontes E. COMSOL Multiphysics®: Finite element software for electrochemical analysis. A mini-review. Electrochem Commun 2014;40:71–74; doi: 10.1016/j.elecom.2013.12.020

49. Pataro G, Barca GM, Ferrari G. Mathematical Modeling of Electrochemical Phenomena at the Electrode-Solution Interface in a PEF Treatment Chamber. In: 1st World Congress on Electroporation and Pulsed Electric Fields in Biology, Medicine and Food & Environmental Technologies. (Jarm T, Kramar P. eds.) IFMBE Proceedings Springer Singapore: Singapore, 2016; pp. 97–100.

50. Nilsson E, Fontes E. Mathematical modelling of physicochemical reactions and transport processes occurring around a platinum cathode during the electrochemical treatment of tumours. Bioelectrochemistry 2001;53(2):213–224; doi: 10.1016/S0302-4598(01)00097-6

51. Mokhtare A, Shiv Krishna Reddy M, Roodan VA, et al. The role of pH fronts, chlorination and physicochemical reactions in tumor necrosis in the electrochemical treatment of tumors: A numerical study. Electrochim Acta 2019;307:129–147; doi: 10.1016/j.electacta.2019.03.148

52. Patel BA. Chapter 1 - Introduction to Electrochemistry for Bioanalysis. In: Electrochemistry for Bioanalysis. (Patel B. ed.) Elsevier: Amsterdam, Netherlands; 2020; pp. 1–8.

53. Guseva O, Schmutz P, Suter T, et al. Modelling of anodic dissolution of pure aluminium in sodium chloride. Electrochim Acta 2009;54(19):4514–4524; doi: 10.1016/j.electacta.2009.03.048

54. Rodaite-Riseviciene R, Saule R, Snitka V, et al. Release of iron ions from the stainless steel anode occurring during high-voltage pulses and its consequences for cell electroporation technology. IEEE Trans Plasma Sci 2014;42(1):249–254; doi: 10.1109/TPS.2013.2287499

55. Turjanski P, Olaiz N, Maglietti F, et al. The role of pH fronts in reversible electroporation. PLoS One 2011;6(4):e17303; doi: 10.1371/journal.pone.0017303

56. Miklavčič D, Serša G, Kryžanowski M, et al. Tumor treatment by direct electric current-tumor temperature and pH, electrode material and configuration. Bioelectrochem Bioenerg 1993;30:209–220; doi: 10.1016/0302-4598(93)80080-E

57. Nilsson E, Berendson J, Fontes E. Development of a dosage method for electrochemical treatment of tumours: A simplified mathematical model. Bioelectrochem Bioenerg 1998;47(1):11–18; doi: 10.1016/S0302-4598(98)00157-3

58. Colombo L, González G, Marshall G, et al. Ion transport in tumors under electrochemical treatment: In vivo, in vitro and in silico modeling. Bioelectrochemistry 2007;71(2):223–232; doi: 10.1016/j.bioelechem.2007.07.001

59. Scuderi M, Dermol-Černe J, Batista Napotnik T, et al. Characterization of experimentally observed complex interplay between pulse duration, electrical field strength, and cell orientation on electroporation outcome using a time-dependent nonlinear numerical model. Biomolecules 2023; 13(5):727; doi: 10.3390/biom13050727

60. Rems L, Ušaj M, Kandušer M, et al. Cell electrofusion using nanosecond electric pulses. Sci Rep 2013;3(1):3382; doi: 10.1038/srep03382

61. Anonymous. Electrochemical Thermodynamics and Kinetics (Landolt-Börnstein: Numerical Data and Functional Relationships in Science and Technology - New Series, 9A) - Holze, Rudolf: 9783540410386 - AbeBooks. n.d. Available from: https://www.abebooks.com/9783540410386/ Electrochemical-Thermodynamics-Kinetics-Landolt-B% C3%B6rnstein-Numerical-3540410384/plp [Last accessed: June 15, 2023].

62. Wahab FMAE, Khedr MGA, Din AMSE. Effect of anions on the dissolution of Al in acid solutions. J Electroanal Chem Interfacial Electrochem 1978;86(2):383–393; doi: 10 .1016/S0022-0728(78)80012-6

63. Picard T, Cathalifaud-Feuillade G, Mazet M, et al. Cathodic dissolution in the electrocoagulation process using aluminium electrodes. J Environ Monit 2000;2(1):77–80; doi: 10.1039/a908248d

64. Sherif E-S. A comparative study on the electrochemical corrosion behavior of iron and X-65 steel in 4.0 wt % sodium chloride solution after different exposure intervals. Molecules 2014;19(7):9962–9974; doi: 10.3390/molecules 19079962

65. Deborde M, Von Gunten U. Reactions of chlorine with inorganic and organic compounds during water treatment— Kinetics and mechanisms: A critical review. Water Res 2008;42(1–2):13–51; doi: 10.1016/j.watres.2007.07.025

Address correspondence to:
Damijan Miklavčič, PhD
Faculty for Electrical Engineering
University of Ljubljana
Tržaška cesta 25
Ljubljana 1000
Slovenia

Email: damijan.miklavcic@fe.uni-lj.si